CIVIL ENGINEERING JOURNAL

Article no. 32

THE CIVIL ENGINEERING JOURNAL 4-2024

EXPERIMENTAL STUDY OF PRESTRESSED STEEL WIRE ROPE-COMPOSITE MORTAR FOR FLEXURAL STRENGTHENING OF RC BEAMS

Xilong Zheng[1] and Honglei Zhang[2]

1. *School of Civil and Architectural Engineering, Harbin University, No.109 Zhongxing Road, Harbin, Heilongjiang Province, China; sampson88@126.com*
2. *Bridge Department, Beijing New Bridge Technology Development Co., LTD, No.8 Xitucheng Road, Beijing, China*

ABSTRACT

This paper proposes a new method for strengthening structures using prestressed steel wire rope-composite mortar. Firstly, the flexural performance test was conducted on reinforced concrete rectangular beams using composite mortar and prestressed steel wire rope. The test included one reference beam and four reinforced beams. The different arrangements of steel wire ropes and the influence of composite mortar on the flexural performance of the beams were analyzed. ANSYS finite element analysis software was used to perform nonlinear numerical simulations of the reinforced and unreinforced beams, and the results of the finite element modeling were compared with the test results to verify the reliability of the experimental findings. By comparing and analyzing the data of deflection, strain, and other parameters before and after strengthening, it was found that the prestressed steel wire rope strengthening method can significantly improve the load-carrying capacity of the existing bridge, greatly improve the structural performance, and have a good effect on resisting cracking in the reinforced concrete beams. The composite mortar can extend the service life of the prestressed steel wire rope and has excellent durability.

KEYWORDS

Prestressed steel wire rope, Strengthening, Prestressed steel wire rope-composite mortar, Experimental study

INTRODUCTION

Highways are important national infrastructure, carrying the responsibility for social and economic development. Bridges are an essential component of highways, and the safety of bridge usage directly affects the smooth operation of the entire route [1-2]. With the vigorous development of the socio-economy, the demand for various goods is increasing, leading to a growing traffic volume. As a result, the traffic density and vehicle load are increasing. Meanwhile, due to the long-term exposure to natural and usage environments, a significant number of bridges are aging rapidly, experiencing severe functional decay, and can no longer meet the requirements for normal vehicle passage [3-5]. Early constructed bridges were designed with low standards, and with the passage of time, concrete material deteriorates and steel reinforcement corrodes, resulting in a reduction in the load-bearing capacity of bridges. These bridges no longer meet the requirements for transportation development [6-8].

Due to the high cost of bridge construction, it would require a substantial amount of funding if all the unsafe bridges were to be demolished and rebuilt. Additionally, the construction of new bridges would also take a significant amount of time [9]. If the bridges that are not suitable for modern traffic can be systematically repaired and reinforced, gradually increasing their load-bearing capacity to meet the usage standards, it would not only extend the service life of the bridges but also reduce the overall investment amount. This approach ensures that the bridges meet the required transportation capacity while avoiding the concentration of financial resources. It would bring significant economic and social benefits to the country [10-15].

Some commonly used methods for bridge reinforcement include steel plate bonding reinforcement, fiber composite material bonding reinforcement, and externally prestressed reinforcement [16-17]. The steel plate bonding reinforcement method involves using adhesive and bolts to directly bond steel plates to the tensioned areas or weak shear zones of the reinforced concrete structure. This creates an integrated and load-bearing system, thus improving the structural capacity. However, the effectiveness of the reinforcement depends on the quality and durability of the adhesive, and there are high requirements for corrosion protection of the steel plates [18]. The fiber composite material bonding reinforcement method involves using adhesive to bond fiber composite materials to the surface of the reinforced components, creating a unified and load-bearing system that enhances the load-carrying capacity and ductility of the components. However, this method poses challenges in calculating the load-carrying capacity, has limited effectiveness in improving the original structural stress condition, and is prone to adhesive failure [19-20]. The externally prestressed reinforcement method involves introducing external prestressing tendons to actively apply external forces to the existing concrete beams, thereby improving the structural stress condition. However, the prestressing tendons are susceptible to damage from external factors, and the anchoring devices are vulnerable to corrosion from atmospheric exposure. Additionally, the construction requirements for anchoring are demanding [21-23].

This article proposes a prestressed steel wire rope-composite mortar reinforcement technique. The prestressed steel wire rope-composite mortar reinforcement technique is a novel method for reinforcing bridge structures. This reinforcement method utilizes small-diameter prestressed steel wire ropes as the medium for applying prestressing forces, which are transmitted to the reinforced structure through anchors and bonded to the main beam using composite mortar. The reinforcement will impact and alter the distribution of internal forces in the original structure, reducing the tensile stress at the bottom of the beam. By applying prestressed steel wire ropes, the main beam will exhibit a certain degree of arching, which unloads the beam and enhances its capacity to resist bending. This technique also reduces the deflection of the main beam under load and has a shrinkage effect on the cracks that occur in the structure under external loading.

TEST MATERIAL

(1) Concrete

The concrete strength grade of the test beam is C30. It is made using ordinary Portland cement, coarse sand, and crushed stones (with a particle size of 16-30 mm constituting 55%, and 10-20 mm constituting 45%). The mix ratio is as follows: cement: sand: crushed stones: water = 377: 690: 1173: 210, with a water-cement ratio (W/C) of 0.57. Alongside the production of the concrete test beam, 15 standard cube specimens measuring 150 mm × 150 mm × 150 mm are precast. After curing under the same conditions as the test beam for 28 days, the compressive strength of the concrete is determined using a compression testing machine. The average compressive strength of the cubes is 35.4 MPa.

(2) Steel

In this experiment, there are three types of steel bars with diameters of φ8, φ12, and φ14. Three bars of each diameter were taken for material mechanical property testing. The measured yield strengths of the steel bars are 360 MPa, 355 MPa, and 370 MPa, respectively. The ultimate strengths are 478 MPa, 509 MPa, and 550 MPa, respectively. The elastic modulus is 2×10^5 MPa.

(3) Steel wire rope

The selected diameter of the prestressed steel wire rope in the experiment is 4 mm. The standard tensile strength is 1670 MPa, the elastic modulus is 1.3×10^5 MPa, and the cross-sectional area is 9.55 mm².

(4) Aluminum alloy casing

In this experiment, the steel wire rope end is pressed with an octagonal hole elliptical aluminum alloy casing, forming a pile head anchor to anchor the steel wire rope to the anchor. The diameter of the casing is determined based on the diameter of the steel wire rope. For this experiment, a casing with an inner diameter of 11 mm, length of 40 mm, and wall thickness of 2 mm was selected. The aluminum casing and extrusion device are shown in Figure 1.

Fig. 1 - Steel wire rope after extrusion molding

(5) Composite mortar

Composite mortar is prepared by mixing modified vinyl acetate emulsion, polymer adhesive powder, cellulose ether, and hard dry powder in certain proportions. It has good workability, is non-toxic and environmentally friendly, and has excellent adaptability to old concrete substrates. It has strong adhesive strength, good waterproofing properties, and provides good protection for reinforced steel. Its 28-day flexural strength is 8.4 MPa, compressive strength is 51.4 MPa, and bond strength is 2.5 MPa.

(6) Anchor equipment

The test beam adopts slotted anchor equipment, which consists of a rectangular groove of 40 mm in length, 5 mm in width, and 10 mm in depth on the anchor block. The 6 slots are evenly distributed on the anchor block. When installing the steel wire rope, one end of the steel wire rope is threaded through the rectangular groove and fixed with an aluminium sleeve. The other end of the steel wire rope is tensioned. The anchor block is made of Q235 steel with an elastic modulus of $E=2\times10^5$ MPa. The dimensions of the inner anchor are 250 mm×40 mm×50 mm, as shown in Figure 2 and Figure 3.

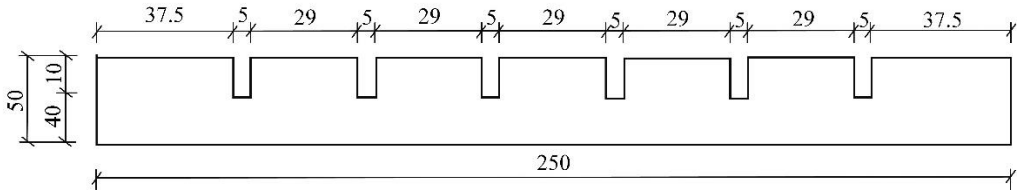

Fig. 2 - Inner grooved anchor fastener elevation diagram (Unit: mm)

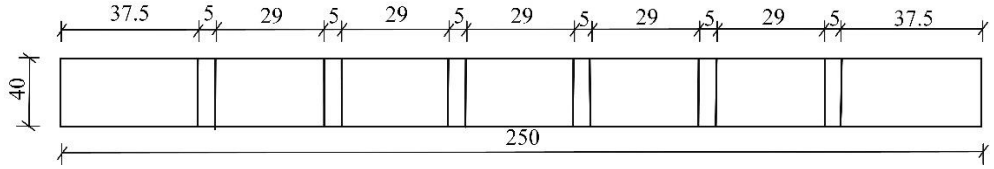

Fig. 3 - Inner grooved anchor fastener plan view (Unit: mm)

EXPERIMENTAL PLAN

Loading Device

In this test, all 5 beams were loaded using a two-point loading method with three equal segments. A 30-ton manual hydraulic jack and reaction frame were used to apply the load, with the load values measured through a pressure sensor connected to the hydraulic jack. The load applied by the hydraulic jack directly acted on the test beams through the distributing beams. The loading device is shown in Figure 4, with L=2600 mm, a=100 mm, b=800 mm, c=800 mm.

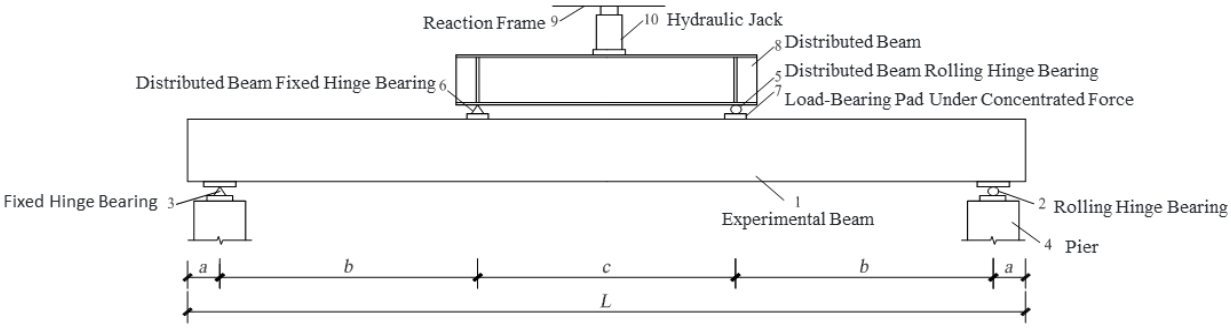

Fig. 4 - Loading device diagram

Loading scheme

During the experiment, a monotonic graded loading strategy was adopted. Prior to the actual loading, a preloading process should be conducted with a preload value of 10-20 kN to ensure the proper functioning of the experimental apparatus and instruments. During the formal loading, each level was loaded with 5 kN. When the load reached 80% of the cracking load, the loading value was reduced to 3 kN per level until the component cracked. After the component cracked, the loading continued at 5 kN per level. When the load approached 90% of the ultimate load, the loading value was reduced again to 3 kN per level. The loading was stopped once the component reached its ultimate state. Each level of loading was held for 15 minutes, and data was collected after the instruments stabilized. The development and width of cracks were also observed.

Test Content and Methodology

(1) Concrete strain testing

Five strain gauges are symmetrically installed along the height of the cross-section at midspan on both sides of the test beam to measure the average strain distribution of the concrete on the side surface of the beam along the section height. The layout of the measurement points is shown in Figure 5.

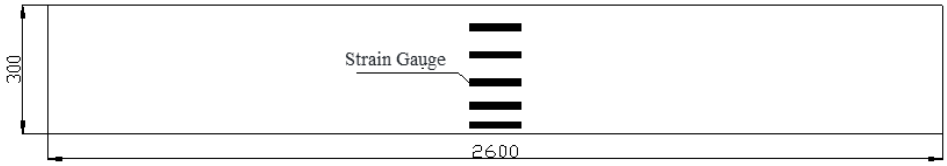

Fig. 5 - Layout diagram of concrete strain measurement points (Unit: mm)

(2) The strain testing of steel reinforcement and steel wire rope.

After the completion of the reinforcement framework binding, resistance strain gauges are arranged at different positions along the longitudinal tensioned steel bars, encapsulated with epoxy resin to prevent damage during the concrete pouring process. For the steel wire ropes, resistance strain gauges are pasted onto them to measure the strain variation. The layout of the steel reinforcement strain gauges is shown in Figure 6.

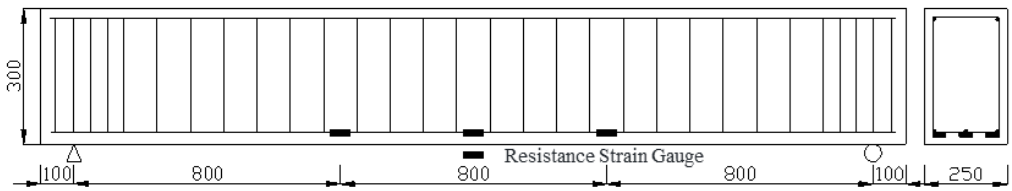

Fig. 6 - Layout diagram of steel reinforcement strain measurement points (Unit: mm)

(3) Deflection test

In the experiment, a displacement sensor is placed at each end of the test beam, at the mid-span position, and at the L/4 position to measure the actual deflection at the mid-span position under different loading levels.

The strain and pressure sensor data for concrete, steel reinforcement, and steel wire ropes, as well as the deflection of the test beam, are collected using the TDS-530 data acquisition instrument. The crack width of the test beam is measured using the PTS-C10 intelligent crack width observer.

Fig. 7 - Loading device diagram

Fig. 8 - Displacement sensor placement diagram

THE PROCESS OF BEAM FAILURE AND CRACK ANALYSIS

The process of beam failure in the experiment

(1) The comparative beam DB0

DB0 is a comparative beam, which was not reinforced in any way for the experimental purpose. When the load was applied up to 18.46 kN, the concrete beam exhibited micro-fine cracks with a vertical length of 7 cm and a width of 0.08 mm. As the load increased to 30 kN, the crack width reached 0.11 mm, with relatively fewer new cracks formed but an increased width of the existing cracks, and they propagated rapidly upwards. When the load reached 87.31 kN, the longitudinal steel reinforcement at the bottom of the beam yielded, and the maximum crack width in the beam reached 1.3 mm. Subsequently, the concrete cracks expanded rapidly, especially near the mid-span section where the concrete in the compression zone failed. The crack width reached 5.8 mm, and the vertical length of the crack along the beam height reached 24 cm. The crack development of the comparative beam is shown in Figure 9, where the numbers indicated the magnitude of the total load applied on top of the beam.

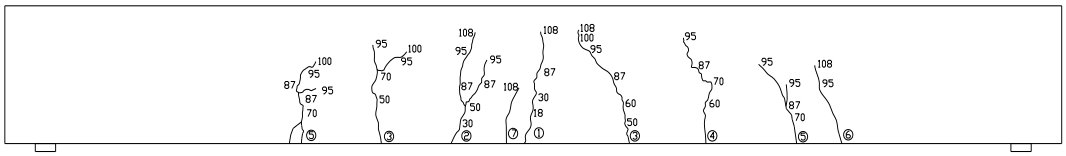

Fig. 9 - Crack distribution diagram of the comparative beam (Unit: kN)

(2) Single-layer reinforced beam JG1

JG1 is a single-layer reinforced beam, with six prestressed steel wires applied at the bottom of the beam. When the load was applied up to 48.83 kN, the concrete in the beam cracked at the corresponding bottom position of the loading point on the distribution beam, with a crack width of 0.07 mm and a vertical length of 4 cm along the beam height. At 60 kN, a second crack appeared at the bottom position of the loading point on the other end of the distribution beam, with a width of 0.07 mm. The width expansion of the first crack was relatively small, and it propagated upwards at a slow rate. At 173.36 kN, the maximum crack width in the tested beam reached 1.82 mm, and the vertical length of the crack along the beam height reached 24 cm. According to the "Standard for Test Methods of Concrete Structures" (GB/T50152-2012), the crack width at the tensile main reinforcement reaching 1.50 mm indicates that the specimen has reached the ultimate limit state (failure) specified in the standard. It can be concluded that the load-carrying capacity of the tested beam has reached the ultimate limit state, and the crack development is shown in Figure 10.

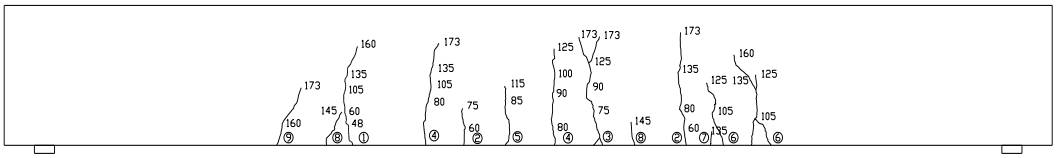

Fig. 10 - Crack distribution diagram of beam JG1 (Unit: kN)

(3) Double-layer reinforced beam JG2

JG2 is a double-layer reinforced beam, with twelve prestressed steel wires applied at the bottom of the beam. When the load was applied up to 69.23 kN, fine cracks appeared at the bottom of the beam, with a crack width of 0.06 mm and a vertical length of 2 cm along the beam height. At 155 kN, diagonal cracks appeared near the anchorages in the shear zone, with larger widths and lengths.

The width of the diagonal crack was 0.82 mm, and the diagonal length was 26 cm. At 219.19 kN, the maximum crack width in the tested beam reached 1.72 mm, with a vertical length of 23 cm. The load reached the ultimate limit state, and the crack development is shown in Figure 11.

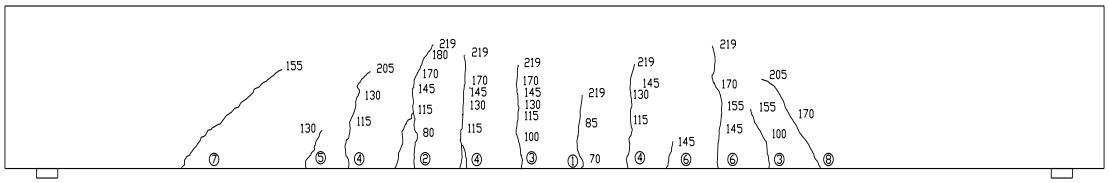

Fig. 11 - Crack distribution diagram of beam JG2 (Unit: kN)

(4) U-shaped reinforced beam JG3.

JG3 is a U-shaped reinforced beam, which is subjected to double-layer prestressed steel wires at the bottom of the beam and an additional layer of three prestressed steel wires on each side of the beam. When the load was increased to 79.95 kN, fine cracks appeared at the bottom of the beam, with a crack width of 0.04 mm and a vertical length of 2 cm along the height of the beam. At 115 kN, the crack width in the concrete reached 0.24 mm, with fewer additional cracks in the beam. At 245.63 kN, the maximum width of the concrete cracks in the test beam reached 1.58 mm, with a vertical length of 19 cm along the height of the beam. The load-bearing capacity reached the ultimate limit state, as shown in Figure 12, depicting the crack development of the JG3 beam.

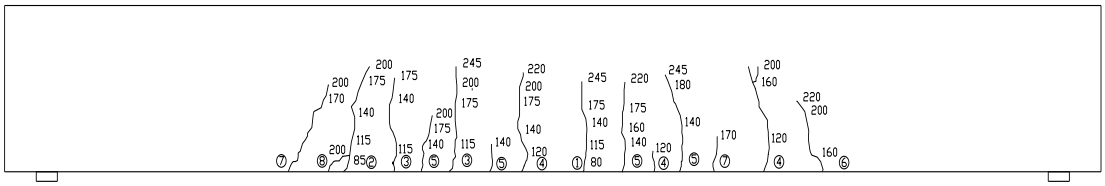

Fig. 12 - Crack distribution diagram of JG3 beam (Unit: KN)

(5) Double-layer reinforced beam JG4.

JG4 is a double-layer reinforced beam with two layers of 12 prestressed steel wires applied at the bottom of the beam and coated with a layer of composite mortar. Due to the shrinkage of the composite mortar during the setting and hardening process, fine cracks have already appeared on the surface of the reinforcement layer before loading. When the load was increased to 73.40 kN, cracks appeared at the bottom of the beam on one side at a distance of 10 cm from the mid-span and on the other side at a distance of 12 cm from the loading point of the distributed beam. The crack widths were 0.06 mm and 0.05 mm respectively, with vertical lengths along the height of the beam of 2 cm and 1cm respectively. At 220.86 kN, the steel wires fractured, and the maximum width of the concrete cracks in the test beam reached 1.61 mm, with a vertical length along the height of the beam of 22 cm. The load-bearing capacity reached the ultimate limit state, as shown in Figure 13, depicting the crack development of the JG4 beam.

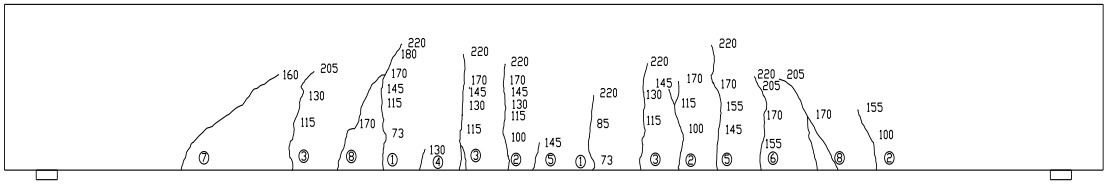

Fig. 13 - Crack distribution diagram of JG4 beam (Unit: kN)

Crack Analysis

The cracks in the reinforced beam exhibit a “fine and dense” characteristic. The crack development in the reinforced beam is slower compared to the reference beam. Under the same load value, the maximum crack width measured in the reference beam is greater than that in the reinforced beam. After yielding of the reinforcement, the crack development in the reinforced beam is relatively slow, while the crack development in the reference beam is rapid.

When the bearing capacity reaches the ultimate limit state, the maximum crack width of the reinforced beam is significantly smaller than that of the unreinforced beam. Additionally, the maximum crack width of beams reinforced with composite mortar is smaller than that of beams without composite mortar reinforcement. When the bearing capacity reaches the ultimate limit state, the unreinforced beam has fewer cracks with larger average spacing. On the other hand, the reinforced beam has a greater number of cracks with smaller average spacing. Among them, the U-shaped reinforced beam has the densest cracks and the smallest crack width.

MAIN EXPERIMENTAL RESULTS AND ANALYSIS

Experimental results

The main experimental results are shown in Table. 1, where P_{cr} represents the cracking load of the concrete beam, P_y represents the load value when the longitudinal steel reinforcement at the bottom of the beam starts yielding, Pu represents the ultimate load-bearing capacity of the concrete beam, Δ_y and Δ_u respectively represent the mid-span deflection values at the yield load and ultimate load. The improvement data of the reinforced beams can be found in Table. 2, where α_{cr}, α_y, and α_u represent the ratios of the cracking load, yield load, and ultimate load of each reinforced beam to the corresponding values of the reference beam DB0.

Tab. 1 - Main experimental results of the test beams

Test specimen number	P_{cr}（kN）	P_y（kN）	P_u（kN）	Δ_y（mm）	Δ_u（mm）
DB_0	18.46	87.31	108.50	6.72	24.29
JG_1	48.83	133.85	173.36	9.18	21.98
JG_2	69.23	171.59	219.19	9.64	21.04
JG_3	79.95	198.45	245.63	9.65	20.23
JG_4	73.40	173.51	220.86	9.58	20.99

Tab. 2 - Translation of the data for the strengthened beams

Test specimen number	α_{cr}	α_y	α_u	Δ_u/Δ_y
DB_0	1.00	1.00	1.00	3.62
JG_1	2.65	1.53	1.60	2.39
JG_2	3.75	1.97	2.02	2.18
JG_3	4.33	2.27	2.26	2.10
JG_4	3.98	1.99	2.04	2.19

Analysis of test results

The cracking load, yield load, and ultimate load of the reinforced beams have all been significantly increased compared to the unreinforced beams. Among them, the JG3 beam has the largest increase, with an improvement of 126% in ultimate load. The JG1, JG2, and JG4 beams have respective increases of 60%, 102%, and 104% in ultimate load. The JG3 beam has a larger increase in ultimate load compared to the JG2 beam, and the JG2 beam has a higher increase compared to the JG1 beam. This indicates that under the same controlled stress of prestressed steel wire rope tension, the reinforcement effect is best with U-shaped arrangement, and the reinforcement effect with a double-layer arrangement is better than a single-layer arrangement.

The yield load and ultimate load of JG2 beam and JG4 beam are similar, indicating that the composite mortar has little influence on the final load-bearing capacity of the beams. However, the cracking load of JG4 beam has increased by 6% compared to JG2 beam, indicating that the beams reinforced with composite mortar have better crack resistance. The strengthened beams show a significant increase in cracking load, indicating that the reinforcement with prestressed steel wire rope has a certain inhibitory effect on crack propagation.

Sectional stiffness analysis

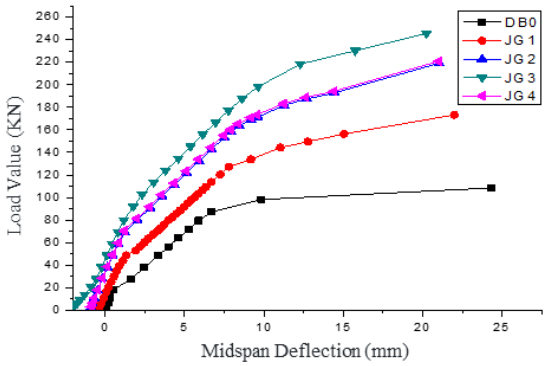

Fig. 14 - Load deflection curve

Tab. 3 - Load value comparison at the same displacement

Test specimen number	$P_{l/400}$ (kN)	$\alpha_{l/400}$	$P_{l/300}$ (kN)	$\alpha_{l/300}$	$P_{l/200}$ (kN)	$\alpha_{l/200}$
DB_0	80.42	1.00	91.83	1.00	99.85	1.00
JG_1	104.80	1.30	128.11	1.40	147.28	1.48
JG_2	132.48	1.65	158.56	1.73	184.76	1.85
JG_3	154.66	1.92	177.19	1.93	215.46	2.16
JG_4	133.97	1.67	160.33	1.75	186.40	1.87

According to the load-deflection relationship curve in Figure 14, it can be observed that before the concrete cracks, the deflection growth of both the reinforced and unreinforced beams is relatively slow. After the concrete cracks, the deflection growth accelerates, and the deflection of the unreinforced beam increases faster than that of the reinforced beam. After the reinforcement steel yields, the deflection of the unreinforced beam increases significantly, while the deflection of the reinforced beam develops slowly in comparison. Among them, the deflection development of the U-

shaped reinforced beam is the slowest, followed by the double-layer reinforced beam and then the single-layer reinforced beam. Table. 3 lists the corresponding load values at mid-span deflections of L/400, L/300, and L/200, where L is the distance between the centers of the beam supports, which is 2400 mm. $\alpha_{l/400}$, $\alpha_{l/300}$, $\alpha_{l/200}$ represent the ratio of the ultimate load capacity at the corresponding mid-span deflections of L/400, L/300, L/200 to the ultimate load capacity of the unreinforced beam (DB0). The $P_{l/400}$ of beam DB0 is 80.42 kN, and the $P_{l/400}$ of beam JG1 is 104.80 kN, which is an increase of 30% compared to beam DB0. The $P_{l/400}$ of beam JG2 and JG4 is 132.48 kN and 133.97 kN, respectively, which is an increase of 65% and 67% compared to the unreinforced beam. The $P_{l/400}$ of beam JG3 is 154.66 kN, which is an increase of 92% compared to the unreinforced beam. The $P_{l/300}$ of beam DB0 is 91.83 kN, and the $P_{l/300}$ of beam JG1 is 128.11 kN, which is an increase of 40% compared to beam DB0. The $P_{l/300}$ of beam JG2 and JG4 is 158.56 kN and 160.33 kN, respectively, which is an increase of 73% and 75% compared to the unreinforced beam. The $P_{l/300}$ of beam JG3 is 177.19 kN, which is an increase of 93% compared to the unreinforced beam. Similar trends can be observed for the load values corresponding to the mid-span deflection of L/200. Through the above comparisons, it can be concluded that prestressed steel strand reinforcement has a significant effect on improving the beam's sectional stiffness. Among them, the U-shaped reinforcement has the most pronounced effect, and the double-layer reinforcement performs better than the single-layer reinforcement. The influence of the composite mortar on the beam's sectional stiffness is negligible. The main reasons for these effects are that the beam undergoes a positive moment redistribution after the steel strands are tensioned, creating prestress in the tensioned zone at the bottom of the beam, which greatly improves the beam's stiffness. The reinforcement steel strands act as additional reinforcement, effectively increasing the reinforcement ratio of the member, thus contributing to the stiffness improvement.

Performing strain analysis

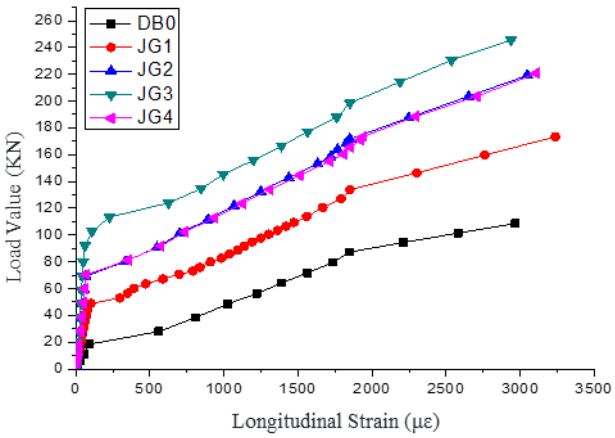

Fig. 15 - Comparison of steel reinforcement strains

Figure 15 compares the strain curves of longitudinal reinforcement at the bottom of the beams at mid-span positions. From the graph, it can be observed that due to the presence of steel strands, the strain development of reinforced beam reinforcement is slower than that of unreinforced beam reinforcement as the load increases. This phenomenon is not very significant at lower load values but becomes more pronounced at higher load values. Among them, the lag in strain development of reinforcement in beam JG3 is more significant than that in beam JG2, and the lag in strain development of beam JG2 is more significant than that in beam JG1. However, there is not much difference in the variation of steel reinforcement strain between beam JG2 and JG4. This indicates that under the same controlled stress of prestressed steel strands, the lag in strain development of

reinforcement is most significant in U-shaped reinforced beams, while the effect of composite mortar on steel reinforcement strain is minimal.

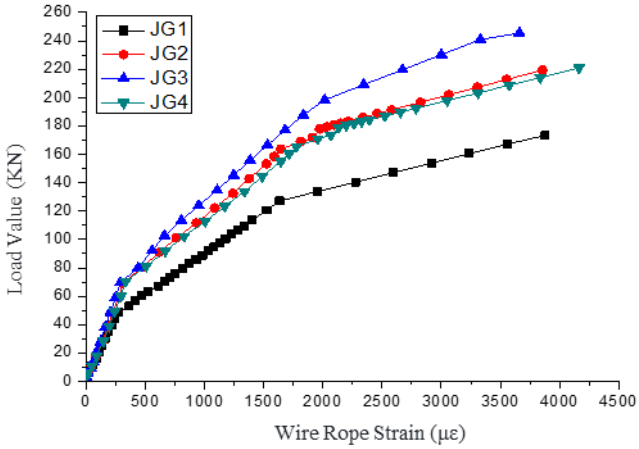

Fig. 16 - Comparison of steel strand strains

Figure 16 shows the load-steel strand strain comparison curves for each reinforced beam. From Figure 16, it can be observed that the steel strand strain changes fastest for beam JG1 as the load value increases, while it changes slowest for beam JG3. This is mainly due to the smaller quantity of steel strands used for reinforcement in beam JG1 and the larger deformation of the beam. The strain curves for beam JG2 and JG4 show a similar trend, but there is a difference because beam JG4 is coated with composite mortar at the bottom, causing the strain to concentrate at the cracks, resulting in a higher maximum strain in the steel strands compared to beam JG2.

Verify the Assumption of a Plane Cross-Section

The variation of concrete strain along the height of the mid-span section, measured at three characteristic load values during the loading process of test beams JG1 and JG4, was used to verify the assumption of a plane cross-section for the reinforced beams. The three characteristic load values correspond to 0.18 times the ultimate load, 0.24 times the ultimate load, and 0.65 times the ultimate load, respectively. As seen from Figure 17 and Figure 18, the section strains of the reinforced beams are generally consistent with the assumption of a plane cross-section.

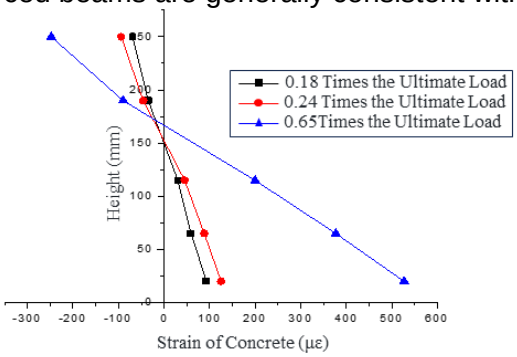

Fig. 17 - Strain distribution along the height of section for beam JG1

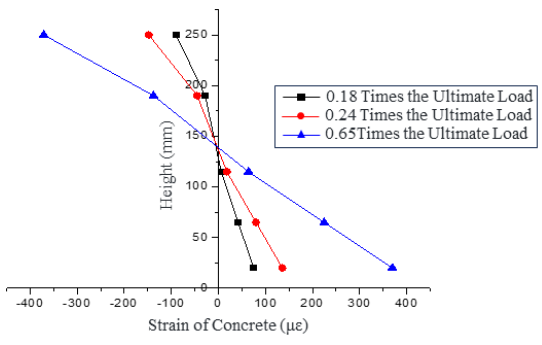

Fig. 18 - Strain distribution along the height of section for beam JG4

FINITE ELEMENT ANALYSIS

Element Selection

The ANSYS program's element library provides various 3D solid elements for simulating three-dimensional solid structures. The elements suitable for concrete in the element library include SOLID 45 (solid element), SOLID 65 (reinforced concrete solid element), SOLID 95 (solid element), and so on, that can be selected. The LINK 8 element is used in the model to simulate reinforced bars and prestressed steel strands, which is a type of beam element. Composite mortar is applied as an external material to the bottom of the test beam. Besides protecting the reinforcement of steel strands used for strengthening, it also ensures the cooperative force transmission between the steel strands and the original components. Similar to the concrete element, the SOLID 65 element can be used to simulate the composite mortar layer. However, due to the thin thickness of the mortar layer (only 3 cm) and its only bearing tensile stress, the model uses the more accurate SHELL 41 element for simulation. The anchors on the bottom surface and side surface of the beam, as well as the pads set at the loading points, are simulated using the SOLID 45 element. The SOLID 45 element is used for the connection between the composite mortar and the beam.

Finite Element Model Establishment

This model simulates a 2.6 m rectangular reinforced concrete test beam. The parameters for concrete, reinforcement, steel strands, and composite mortar are shown in Table. 4.

Tab. 4 - Material parameter table

Material Name	Elastic modulus (MPa)	Poisson's ratio	Specific gravity (kg/m^3)	Cross-sectional area (m^2)
C30 concrete	$3e^4$	0.2	2500	
Steel	$2e^5$	0.3	7800	$1.54e^{-4}$
Steel wire rope	$1.3e^5$	0.3	7800	$9.55e^{-6}$
Composite mortar	$3e^4$	0.3	2500	

The concrete of the beam in the model is implemented using SOLID 65 elements, while the reinforcement and steel wire rope are modeled using LINK 8 elements. The anchors and pads are represented using SOLID 45 elements, and the composite mortar is implemented using SHELL 41 elements. In order to create a pure bending state at the mid-span, the beam is subjected to loading using a two-point loading method with equal divisions. Since the structure is simply supported, the bottom support is located 100 mm away from the beam end and is subjected to linear constraints. After dividing the structure into grids, the finite element model is illustrated in Figure 19 - Figure 20.

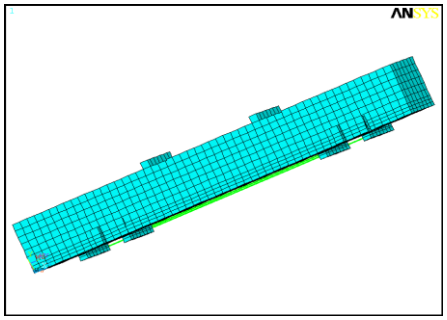

Fig. 19 - Finite element model of anchors and steel wire rope

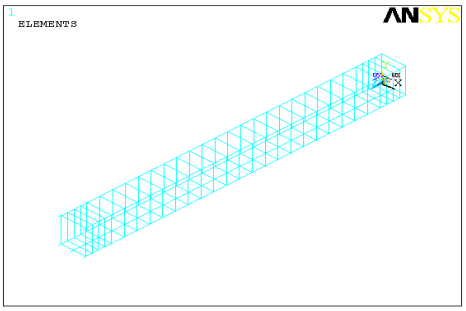

Fig. 20 - Finite element model of reinforcement

Comparing ANSYS analysis results with experimental results

By performing calculations on the established finite element model, characteristic load values, theoretical deflection values, and theoretical strain values of each beam segment can be obtained. By comparing the theoretical values with the experimental values, the accuracy of the finite element analysis results can be mutually validated with the indoor experimental results.

(1) Comparative analysis of theoretical cracking load and yield load with experimental values.

Tab. 5 - Comparative analysis of theoretical and experimental values for cracking load and yield load

Specimen number	Theoretical cracking load/kN	Measured cracking load/kN	Theoretical yield load/kN	Measured yield load/kN
DB_0	17.25	18.46	85.59	87.31
JG_1	46.50	48.83	128.70	133.85
JG_2	67.88	69.23	166.59	171.59
JG_3	77.63	79.95	189.00	198.45
JG_4	71.96	73.40	168.46	173.51

Tab. 6 - Comparative analysis of theoretical and experimental values for cracking load and yield load

Specimen number	Theoretical cracking load ratio	Experimental cracking load ratio	Theoretical yield load ratio	Experimental yield load ratio
DB_0	1	1.07	1	1.02
JG_1	1	1.05	1	1.04
JG_2	1	1.02	1	1.03
JG_3	1	1.03	1	1.05
JG_4	1	1.02	1	1.03

By comparison, it can be seen that the maximum difference between the theoretical and experimental values of cracking load is 7%, and the maximum difference for yield load is 5%. This indicates that the indoor test results are relatively accurate compared to the calculated results from the model. The larger difference in the experimental value of cracking load is mainly due to the visual observation of crack occurrence during the test, which is prone to errors. The cracking load may have been measured after the first crack appeared, leading to larger experimental values. As for the

yield load, the main reason for the larger experimental values is that the concrete grade and the yield strength of steel bars used in the test beam are greater than the design values. Therefore, the experimental values are larger.

(2) Comparison between theoretical deflection and experimental deflection.

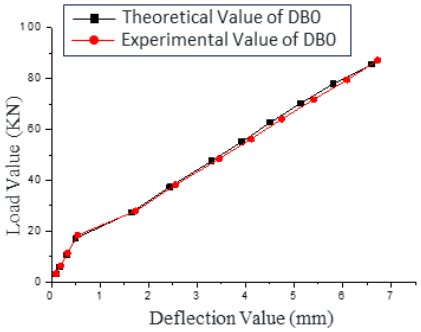

Fig. 21 - Comparison between theoretical deflection and experimental deflection of DB0 beam

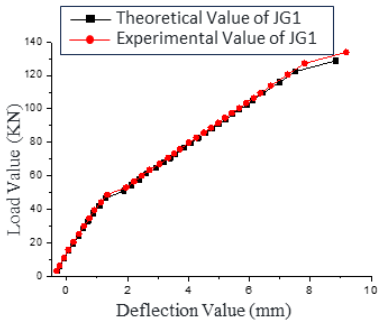

Fig. 22 - Comparison between theoretical deflection and experimental deflection of JG1 beam

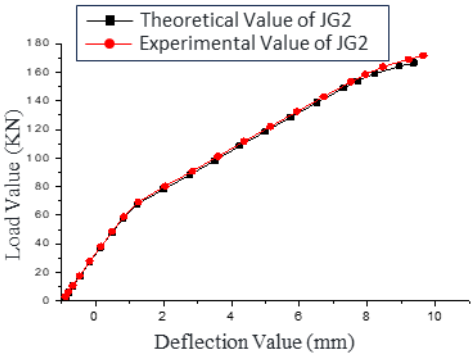

Fig. 23. Comparison between theoretical deflection and experimental deflection of JG2 beam

Figure 21- Figure 24 illustrate the comparison between the experimental and modeled load-deflection curves for DB0, JG1, and JG2 beams (with deflection compared before the yield of steel reinforcement). From the figures, it is observed that there exists some deviation between the experimental results and numerical simulations primarily due to the deviations in the constitutive relationships of concrete and steel reinforcement in the model compared to the actual conditions. However, the theoretical deflection curves and the measured deflection curves from the experiments exhibit consistent trends and demonstrate a high level of fitting, indicating precise experimental results. This also implies that finite element programs can be utilized for simulating and analyzing reinforcement systems in strengthening projects, as they are capable of accurately reflecting the load-bearing behavior of beams.

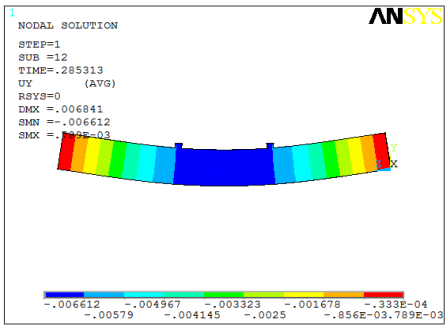

(a) DB0 beam

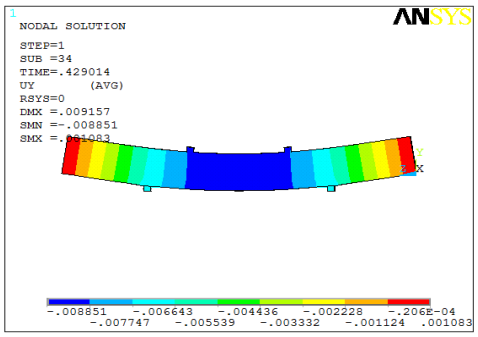

(b) JG1 beam

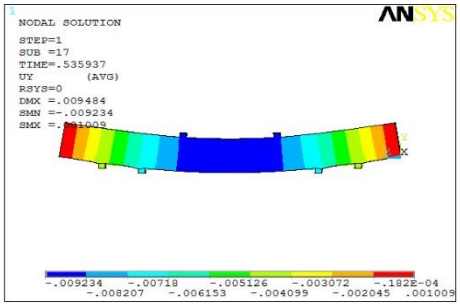

(3) JG2 beam

Fig. 24 - Vertical displacement distribution of the beam under yield condition (Unit: m)

CONCLUSION

The effect of different arrangements of prestressed steel wire ropes and composite mortar on the flexural strengthening of simply supported reinforced concrete beams was studied through indoor experimental tests. By comparative analysis, the following conclusions were drawn:

(1) Prestressed steel wire rope strengthening technology can effectively improve the cracking load, yield load, and ultimate load of the original beam. The beams strengthened with prestressed steel wire ropes have respective increases of 60%~ 104% in ultimate load. Among them, the U-shaped arrangement has the best strengthening effect, the double-layer arrangement has a better effect than the single-layer arrangement.

(2) Prestressed steel wire rope strengthening significantly improves the stiffness of the beam cross-section, with U-shaped reinforcement showing the most pronounced effect. On the other hand, the impact of composite mortar on the beam cross-section stiffness is minimal. The $P_{l/400}$ of beam JG2 and JG4 is 132.48 kN and 133.97 kN, respectively, which is an increase of 65% and 67% compared to the unreinforced beam

(3) After the application of composite mortar prestressed steel wire rope strengthening, the development of strain in the beam reinforcement is slower compared to the unreinforced beam. The loss of prestress in the composite mortar prestressed steel wire rope strengthening technique is primarily caused by the progressive stressing of the steel wire ropes and the relaxation of steel wire rope stress.

(4) The composite mortar prestressed steel wire rope strengthening technique provides effective constraint on the crack development in the beam. The cracks in the strengthened beam exhibit a "fine and dense" characteristic, and the experimental values align well with the calculated values of the cracking load and ultimate load.

REFERENCES

[1] Siwowski T, Piątek B, Siwowska P, et al. Development and implementation of CFRP post-tensioning system for bridge strengthening[J]. Engineering Structures, 2020, 207: 110266.
[2] Hall P. Building bridges: Strengthening the principal induction process through intentional mentoring[J]. Phi Delta Kappan, 2008, 89(6): 449-452.
[3] Crawford B, Soto R, Lemus-Romani J, et al. Investigating the efficiency of swarm algorithms for bridge strengthening by conversion to tied-arch: A numerical case study on San Luis bridge[J]. Iranian Journal of Science and Technology, Transactions of Civil Engineering, 2021, 45: 2345-2357.
[4] Miller T C, Chajes M J, Mertz D R, et al. Strengthening of a steel bridge girder using CFRP plates[J]. Journal of bridge engineering, 2001, 6(6): 514-522.
[5] Williams G, Al-Mahaidi R, Kalfat R. The West Gate Bridge: Strengthening of a 20th century bridge for 21st century loading[J]. Special Publication, 2011, 275: 1-18.
[6] Cardinale G, Orlando M. Structural evaluation and strengthening of a reinforced concrete bridge[J]. Journal of Bridge Engineering, 2004, 9(1): 35-42.
[7] Hu W, Li Y, Yuan H. Review of experimental studies on application of FRP for strengthening of bridge structures[J]. Advances in Materials Science and Engineering, 2020, 2020: 1-21.
[8] Martín-Sanz H, Tatsis K, Damjanovic D, et al. Getting more out of existing structures: steel bridge strengthening via UHPFRC[J]. Frontiers in Built Environment, 2019, 5: 26.
[9] Lopez A, Galati N, Alkhrdaji T, et al. Strengthening of a reinforced concrete bridge with externally bonded steel reinforced polymer (SRP)[J]. Composites Part B: Engineering, 2007, 38(4): 429-436.
[10] Grayson-Wallace B, Aljasar A, Cheng L, et al. Advances in Shear Strengthening of Concrete Bridge Girders[J]. Journal of Bridge Engineering, 2022, 27(6): 03122002.
[11] Chajes M, Rollins T, Dai H, et al. Report on techniques for bridge strengthening: Main report[R]. United States. Federal Highway Administration. Office of Infrastructure, 2019.
[12] Pang B, Yang P, Wang Y, et al. Life cycle environmental impact assessment of a bridge with different strengthening schemes[J]. The International Journal of Life Cycle Assessment, 2015, 20: 1300-1311.
[13] Schnerch D, Dawood M, Rizkalla S, et al. Proposed design guidelines for strengthening of steel bridges with FRP materials[J]. Construction and building materials, 2007, 21(5): 1001-1010.
[14] Zampieri P, Simoncello N, Gonzalez-Libreros J, et al. Evaluation of the vertical load capacity of masonry arch bridges strengthened with FRCM or SFRM by limit analysis[J]. Engineering Structures, 2020, 225: 111135.
[15] Yang J, Hou P, Pan Y, et al. Shear behaviors of hollow slab beam bridges strengthened with high-performance self-consolidating cementitious composites[J]. Engineering Structures, 2021, 242: 112613.
[16] Eberline D K, Klaiber F W, Dunker K. Bridge strengthening with epoxy-bonded steel plates[J]. Transportation Research Record, 1988, 1180: 7-11.
[17] Jasieńko J, Nowak T P. Solid timber beams strengthened with steel plates–Experimental studies[J]. Construction and Building Materials, 2014, 63: 81-88.
[18] Peng J, Tang H, Zhang J. Structural behavior of corroded reinforced concrete beams strengthened with steel plate[J]. Journal of Performance of Constructed Facilities, 2017, 31(4): 04017013.
[19] Hu W, Li Y, Yuan H. Review of experimental studies on application of FRP for strengthening of bridge structures[J]. Advances in Materials Science and Engineering, 2020, 2020: 1-21.
[20] El-Mihilmy M T, Tedesco J W. Analysis of reinforced concrete beams strengthened with FRP laminates[J]. Journal of Structural Engineering, 2000, 126(6): 684-691.
[21] Kim S H, Park J S, Jung W T, et al. Strengthening Effect of the External Prestressing Method That Simulated a Deterioration Bridge[J]. Applied Sciences, 2021, 11(6): 2553.
[22] Kim S H, Park J S, Jung W T, et al. Experimental study on strengthening effect analysis of a deteriorated bridge using external prestressing method[J]. Applied Sciences, 2021, 11(6): 2478.
[23] Madaj A, Mossor K. Evaluation of external prestressing as a strengthening method for existing concrete bridges[J]. Structural Engineering International, 2019, 29(3): 412-416.